Applied Catalysis B: Environmental 183 (2016) 224–230

Contents lists available at ScienceDirect

Applied Catalysis B: Environmental

journal homepage: www.elsevier.com/locate/apcatb

A highly efficient $BiVO_4/WO_3/W$ heterojunction photoanode for visible-light responsive dual photoelectrode photocatalytic fuel cell

Ligang Xia [a], Jing Bai [a], Jinhua Li [a], Qingyi Zeng [a], Xuejin Li [a], Baoxue Zhou [a,b,*]

[a] School of Environmental Science and Engineering, Shanghai Jiao Tong University, No. 800 Dongchuan Rd., Shanghai, China
[b] Key Laboratory of Thin Film and Microfabrication Technology, Ministry of Education, Shanghai 200240, China

ARTICLE INFO

Article history:
Received 21 July 2015
Received in revised form
30 September 2015
Accepted 27 October 2015
Available online 31 October 2015

Keywords:
$BiVO_4/WO_3$ heterojunction
Tungsten substrate
Photocatalytic fuel cell (PFC)
Organic compounds degradation
Electricity generation

ABSTRACT

A highly efficient $BiVO_4/WO_3/W$ heterojunction photoanode was fabricated based on the nanoporous WO_3 film, which was prepared on the tungsten plate by anodic oxidation, in order to facilitate the electrons transfer from $BiVO_4$ to WO_3 by providing a natural connection between WO_3 film and W substrate. Then, a visible-light responsive dual photoelectrode photocatalytic fuel cell (PFC) consisted of $BiVO_4/WO_3/W$ photoanode and Pt modified commercial buried junction silicon (Pt/BJS) photocathode was constructed. The results showed that the optimized $BiVO_4/WO_3/W$ photoanode obtained a photocurrent of 2.01 mA/cm^2 at 0.6 V (vs Ag/AgCl) in 0.1 M KH_2PO_4 (pH 7) electrolyte under simulated AM1.5 solar light, which was 180% and 205% higher than that of bare WO_3 film and bare $BiVO_4$ film, respectively. The established dual photoelectrode PFC showed high converting performance of organics into electricity. For example, a short-circuit current density of 0.26 mA cm^{-2}, which is higher than most of the reported visible-light responsive dual photoelectrode PFC systems, was obtained with the open-circuit voltage of 0.78 V and maximum power output of 2.0×10^{-4} W cm^{-2} in 20 mg L^{-1} tetracycline hydrochloride. Furthermore, a removal ratio of 78% after 4 h was achieved with a stable output photocurrent in the degradation process.

1. Introduction

With the fast development of industries in recent years, large amounts of organic waste discharged into water bodies have caused serious environmental pollution. In view of this, seeking effective purification approach to maintain a green ecological environment is urgent. Furthermore, it would be much promising to develop a new method to eliminate pollutions and simultaneously recover the abundant chemical energy stored in organic wastewater [1–3]. Photocatalytic fuel cell (PFC), a newly developed device for wastewater treatment with simultaneous electricity generation under sunlight, is attracting ever-increasing attention. In such a system, the electrons of the photoanode created under illumination transfer from the external circuit to the cathode to be consumed and at the same time, the holes of photoanode are released for organic compounds degradation.

The PFC systems based on the TiO_2 photoanode have been successfully demonstrated [4–8]. However, the reported systems are still severely limited by poor power generation capacity and wastewater treatment efficiency because TiO_2 photoanode only responds to the UV light. Many studies have attempted to overcome the drawback by coupling with narrow-band gap semiconductors [9–12], but the modified materials are usually unstable in water upon illumination. Thus, several visible light responsive semiconductors such as WO_3 and Fe_2O_3 have been tried to replace TiO_2 photoanode in the PFC [13–17]. However, WO_3 also suffers from weak visible-light absorbance (<460 nm) and a gradual loss of photoactivity during long-term use due to the accumulation of peroxo species on the surface [10,18], and Fe_2O_3 possesses poor charge transport property [19–20]. Therefore, developing stable and highly efficient visible light responsive photoanodes for PFC system is imperative.

$BiVO_4$ has been identified as one of the most promising photoanode materials due to its excellent stability against photocorrosion and small band gap of 2.4 eV that permits efficient light absorption. However, it still suffers from poor charge transport property and excessive electron-hole recombination [21]. Therefore, various strategies such as doping and construction of composite structures have been developed to alleviate the limitation. In contrast to the limited outcome resulted from doping [22], coupling with other

* Corresponding author. Tel.: +86 21 5474 7351; fax: +86 21 5474 7351.
E-mail address: zhoubaoxue@sjtu.edu.cn (B. Zhou).

http://dx.doi.org/10.1016/j.apcatb.2015.10.050
0926-3373/

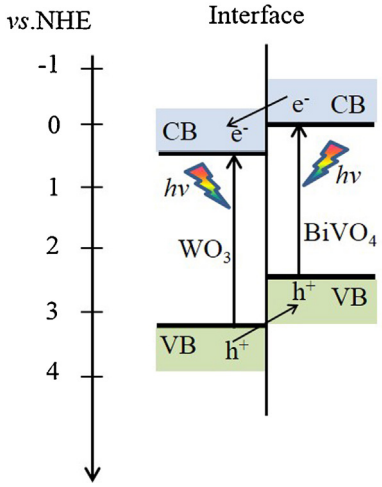

Fig. 1. The deduced relative band positions for the $BiVO_4/WO_3$ heterojunction.

metal oxide semiconductors, including TiO_2 [23], SnO_2 [24–25], $CaFe_2O_4$ [26], WO_3 and ZnO [27–28], to form composite heterojunction has been recognized as an attractive method to develop a high efficiency photoanode material since the composite heterojunction can combine merits and overcome shortcomings of each component. Among them, WO_3 was the most frequently used semiconductor to couple with $BiVO_4$ [29–36] for the proper position of its conduction band (CB) edge (+0.41 V vs. RHE), which allows for facile electron injection from the CB of $BiVO_4$ (+0.02 V vs. RHE), as shown in Fig. 1. Several $BiVO_4/WO_3$ heterojunction photoanodes on conductive glass substrate have been reported. The reported results show that the morphology and structure of the WO_3 under-layer are important factors affecting the performance of the heterojunction and that various structures of WO_3 under-layer on the conductive glass were examined in order to obtain high-quality electron transfer from $BiVO_4$ to conductive glass substrate.

The nanoporous WO_3 film, prepared by anodization on tungsten plate, possesses orderly structures on the tungsten and natural connection between WO_3 and W substrate. Compared with conductive glass substrate, the homogenous and natural connection should not only provide strong connection between the WO_3 film and conductive W substrate to maintain the mechanical flexibility and stability, but also facilitate photogenerated electrons separation and transfer from $BiVO_4$ to WO_3 then to W substrate. However, the $BiVO_4/WO_3$ heterojunction photoanode prepared using a nanoporous WO_3 film as substrate has never been reported.

In this paper, a $BiVO_4/WO_3$ heterojunction photoanode based on the nanoporous WO_3/W film was reported. The optimized photoanode showing excellent photoelectrocatalytic properties was coupled with Pt modified commercial buried junction silicon (Pt/BJS) photocathode to form a visible-light responsive dual photoelectrode PFC, which can improve solar light utilization efficiency compared with single photoelectrode PFC and showed high converting performance of organics into electricity in this study.

2. Experimental

2.1. Preparation of photoelectrodes

The tungsten sheets (0.25 mm thick, 99.9% purity) were cut into samples of 35 mm × 20 mm in size, and then degreased by sonicating in 1:1 acetone and ethanol, followed by rinsing with DI water and drying in a nitrogen stream. The WO_3/W nanoporous electrode was prepared by an electrochemical anodic oxidation method in which tungsten sheet served as anode and platinum foil as cathode. In a typical process, the preparation was conducted in a mixture solution of 0.2 wt% NaF and 0.3% HF at 60 V for 1 h and subsequently at 40 V for 30 min at room temperature using a DC power supply (TRADEX MPS305, 0–60 V). After the electrochemical treatment, the anodized samples were crystallized by annealing at 450 °C for 3 h with heating and cooling rates of 1 °C/min. Next, a solution containing 300 mM bismuth and vanadium prepared by dissolving bismuth nitrate pentahydrate and ammonium metavanadate in 2 mol L^{-1} nitric acid aqueous solution was spin-coated on the nanoporous WO_3/W film. For each layer of coating, the sample was annealed in the air at 450 °C for 20 min on a hot plate. And the last step was to anneal the samples at 450 °C in the furnace for 3 h with heating and cooling rates of 1 °C/min.

Pt/BJS photocathode was prepared according to our previous reports [15] with certain modification. The crystalline silicon photovoltaic cell (PVC), provided by Z.T Solar Technology Co., Ltd. (Guangzhou, China), was cut into samples of 60 mm × 23 mm in size. The backside Al ohmic metal of the PVC was first soldered with a Cu wire which functioned as connecting line and then sealed by the insulating epoxy resin. The Pt decorated PVC (Pt/PVC) was carried out using three-electrode system with platinum foil as the counter electrode, Ag/AgCl as reference and the PVC as the working electrode and prepared by an electrodeposition process in a solution of 1 mM K_2PtCl_6 and 0.1 mol L^{-1} K_2SO_4 (adjusted to pH 1 with H_2SO_4) at −0.5 V (vs Ag/AgCl) under natural sunlight.

2.2. Characterization of photoelectrodes and the established PFC systems

X-ray diffractometry (XRD; AXS-8 Advance, Bruker, Germany) was used to determine the crystal phase of the prepared samples. The morphologies of the samples were studied using a field emission scanning electron microscope (Nova NanoSEM NPE218). The UV–visible absorption spectra of the samples were recorded on a UV–vis photospectrometer (TU-1901, Beijing Purkinje General Instrument Co.).

A 350 W xenon lamp (Shanghai Hualun Bulb Factory) was used as simulated solar light source, and without further description, all experiments were carried out under AM1.5 (light density, 100 mW cm^{-2}) solar light illumination. A solution with 0.1 M KH_2PO_4 (pH 7) was used as the electrolyte. The linear sweep voltammograms (LSV) of photoelectrodes were tested in a rectangular shaped quartz reactor using a three-electrode system with platinum foil as the counter electrode, Ag/AgCl as reference and the prepared photoelectrode as the working electrode. The working electrode potential and current were controlled by using an electrochemical workstation (CHI 660c, CH Instruments Inc., USA). The PFC was assembled using two electrode configurations. The open-circuit voltage (V_{oc}) and short-circuit current (J_{sc}) density of the PFC systems were achieved by using a CHI electrochemical analyzer (CHI 660c, CH Instruments Inc., USA) in two-electrode system. The current–voltage characteristics of PFC were collected with −1.0 V initial potential and +0.2 V final potential at a scan rate of 20 mV s^{-1} and during the test, the photoanode served as the working electrode and the photocathode as the reference and counter electrodes. The organic compounds degradation experiment was performed under the following conditions: moderate stirring, 0.1 mol L^{-1} sodium sulphate as electrolyte, 25 mL reaction solution, and a 1 cm^2 illumination area for both the Pt/BJS photocathode and $BiVO_4/WO_3$/W photoanode. The degradation rate was analyzed with a spectrophotometer (UV2102 PCS, UNICO, Shanghai) at wavelength of 357 nm. All runs were repeated at least three times to check their reproducibility.

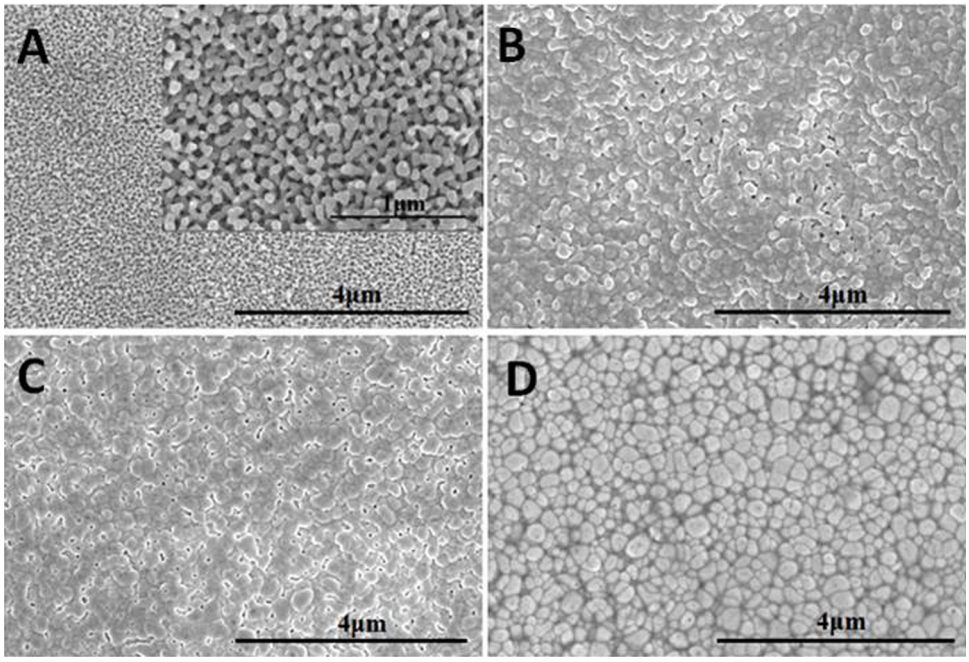

Fig. 2. The top-view SEM images of (A) nanoporous WO_3/W (the inset is a high-magnification SEM image and the scale bar is 1 μm) and nanoporous WO_3/W film coated by different layers of $BiVO_4$: (B) two layers, (C) four layers, (D) six layers. The scale bars are all 4 μm except the inset in (A).

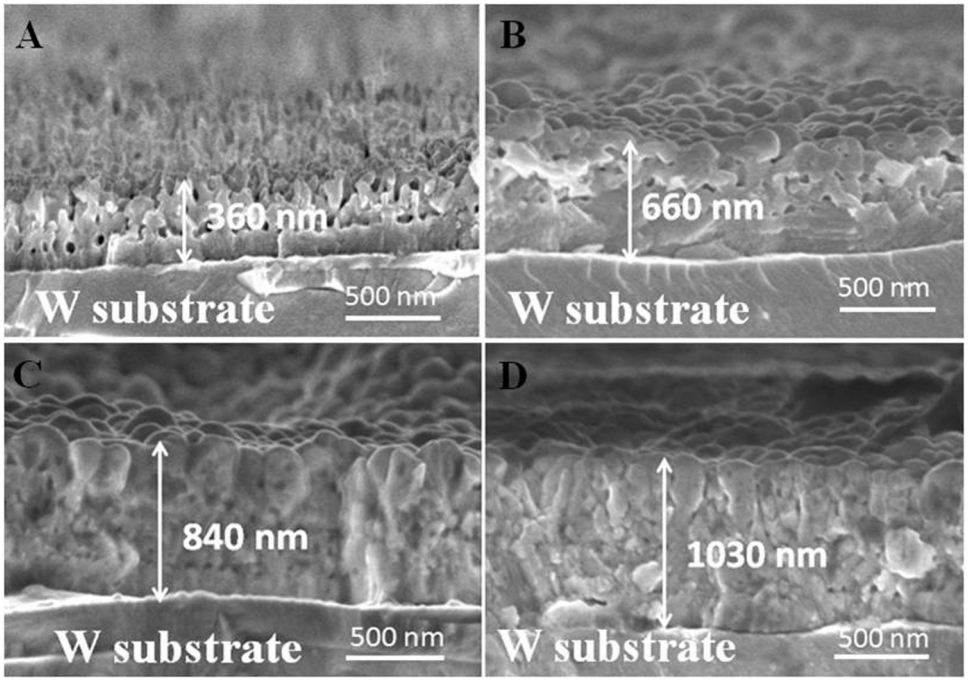

Fig. 3. The cross sectional SEM images of (A) nanoporous WO_3/W, and nanoporous WO_3/W film coated by different layers of $BiVO_4$: (B) two layers, (C) four layers, (D) six layers. The scale bars are all 500 nm.

3. Results and discussion

3.1. The characterizations of photoelectrodes

Fig. 2 shows the top-view scanning electron microscope (SEM) images of the WO_3/W and $BiVO_4$/WO_3/W photoanodes, and Fig. 3 illustrates the corresponding cross sectional SEM images. As seen from Fig. 2A, regular self-assembled nanoporous tungsten oxide structures were formed over the entire surface after the anodization treatment. From the higher resolution SEM image as shown in the insert of Fig. 2A, an intricate nanopore structure with a pore size of dozens of nanometers in diameter could be observed. After being modified by $BiVO_4$, the nanoporous structures were filled and as the number of coating layers increased, more and larger $BiVO_4$ crystals could be seen and the thickness of the $BiVO_4$ film increased (Fig. 3B–D).

Fig. 4 shows the XRD patterns of the WO_3/W film and $BiVO_4$/WO_3/W heterojunctions (with different layers of $BiVO_4$). According to the characteristic diffraction peaks of (200) and (002), the nanoporous WO_3 can be determined as monoclinic WO_3

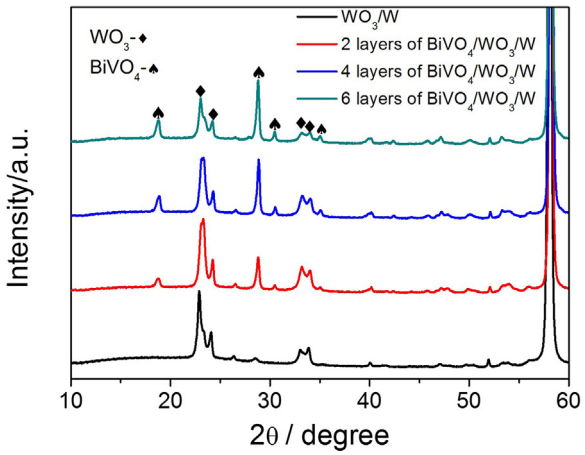

Fig. 4. XRD patterns of nanoporous WO_3/W film and WO_3/W film coated by different layers of $BiVO_4$.

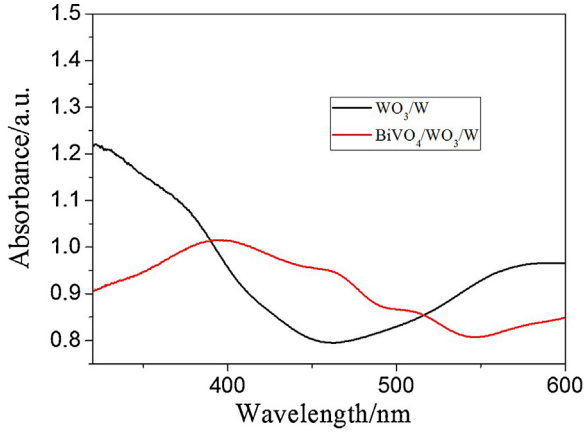

Fig. 5. The UV–vis absorption spectra of nanoporous WO_3/W film and WO_3/W film coated by four layers of $BiVO_4$.

[18]. After the deposition of $BiVO_4$ layer, new peaks appeared at $2\theta = 18.9^\circ$, 28.8°, 30.5° and 35.2°, which correspond to the characteristic diffraction peaks of monoclinic $BiVO_4$ [37], and their intensities increased with the increase of $BiVO_4$ layers. As the coating number increased, the relative content of WO_3 decreased and then the intensity of its characteristic diffraction peaks became slightly lower. The optical behaviors of the WO_3/W film and WO_3/W film coated by four layers of $BiVO_4$ were characterized by UV–vis absorbance spectra as shown in Fig. 5. The light absorption of the WO_3/W film started at around 460 nm and the absorption range of the WO_3/W film was enhanced by the coupling of $BiVO_4$ that has a smaller band gap energy. For the $BiVO_4/WO_3$/W film, the band absorption edges shifted to 545 nm and the absorption intensity was higher than that of the WO_3/W film in the wavelength range of 390–515 nm.

3.2. Photoelectrochemical properties of photoelectrodes

Fig. 6 gives the current-potential plots of $BiVO_4$, nanoporous WO_3/W film and $BiVO_4/WO_3$/W photoanodes under AM1.5 illumination. The photocurrent density of WO_3/W film was 0.72 mA cm^{-2} at 0.6 V (vs Ag/AgCl). The WO_3/W film coated by four layers of $BiVO_4$ exhibited the highest photocurrent density of 2.01 mA cm^{-2} at 0.6 V (vs Ag/AgCl) and showed 180% and 205% higher photoactivity compared with bare WO_3 and bare $BiVO_4$ film, respectively. However, the photocurrent density of $BiVO_4/WO_3$/W photoanode decreased with further increase of $BiVO_4$ layers. When the coating number of $BiVO_4$ increased to six, the photocurrent density decreased dramatically to 0.71 mA cm^{-2} at 0.6 V (vs Ag/AgCl). These results clearly indicate that proper modification of nanoporous WO_3 with $BiVO_4$ effectively reduces the recombination of electrons and holes generated in the nanoporous WO_3 and $BiVO_4$ film, which can be ascribed to the formation of the heterojunction and excellent electron transport between WO_3 film and the tungsten substrate. When less $BiVO_4$ layers were coated, the light absorption range and intensity of $BiVO_4/WO_3$/W photoanode were improved and the photo-generated electrons of $BiVO_4$ film could easily transfer to the nanoporous WO_3, thereby creating higher photocurrent density. But when the $BiVO_4$ layers grew thicker, the photo-generated electrons could no longer easily transfer across the thicker $BiVO_4$ film to the nanoporous WO_3 and they ended up recombining with the holes in a very short time due to poor electron transfer property of $BiVO_4$ film. Moreover, it can be seen from the current-time (I–t) curve of $BiVO_4/WO_3$/W photoanode with four layers of $BiVO_4$ at 0.6 V bias vs. Ag/AgCl reference electrode (Fig. 5, inset), the photocurrent density was about 2 mA cm^{-2} without any significant decrease after 10 min, which indicates that the $BiVO_4/WO_3$/W electrode can be employed as an effective visible-light responsive photoanode that has a long service life.

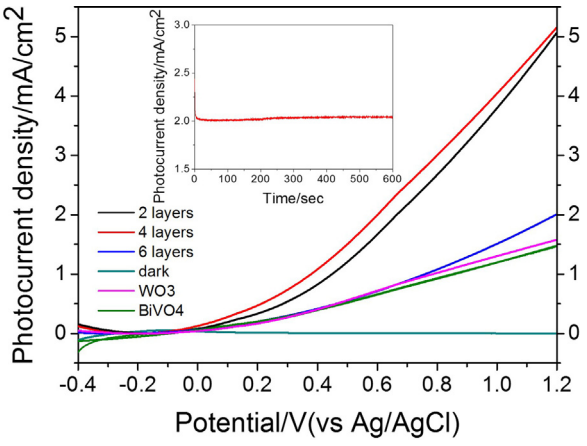

Fig. 6. The LSV plots of $BiVO_4$ film, nanoporous WO_3/W film and WO_3/W film coated by different layers of $BiVO_4$ in 0.1 M KH_2PO_4 solution (pH 7) under AM 1.5 (100 mW cm^{-2}) illumination. Inset: the typical I–t curve of $BiVO_4/WO_3$/W photoanode with four layers of $BiVO_4$ at 0.6 V bias vs. Ag/AgCl reference electrode.

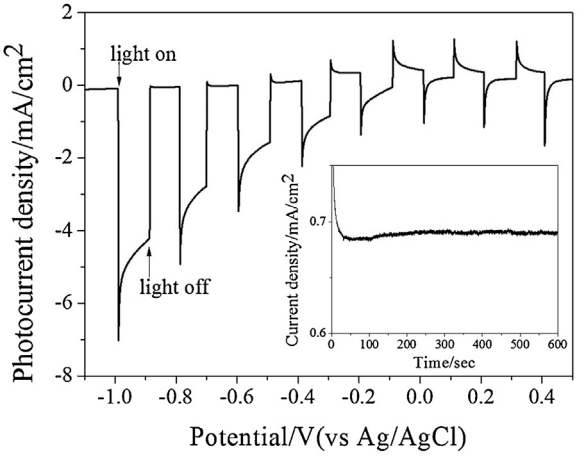

Fig. 7. Chopped LSV curves of Pt/BJS photocathode in 0.1 M KH_2PO_4 solution adjusted to pH 7 under AM 1.5 (100 mW cm^2) illumination, inset: typical I–t curve of Pt/BJS photocathode at −0.2 V bias vs. Ag/AgCl reference electrode tested under the same condition.

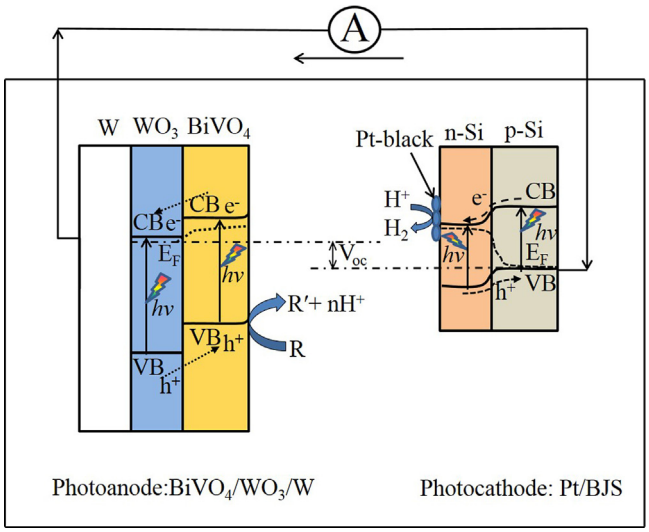

Fig. 8. The energy level diagram of the PFC system comprising the $BiVO_4/WO_3$/W photoanode and Pt/BJS photocathode.

Fig. 7 shows the chopped LSV curve of Pt/BJS photocathode in 0.1 M KH_2PO_4 solution (pH 7) under AM 1.5 illumination. The Pt/BJS photocathode showed an instant photoresponse under illumination. The typical *I*–*t* curve of Pt/BJS photocathode in neutral solutions at −0.2 V bias vs. Ag/AgCl reference electrode (inset in Fig. 7) shows that the photocurrent density did not decrease after 10 min, which confirms the stability and durability of Pt/BJS photocathode for practical applications.

3.3. Characterizations of the established PFC systems

Based on the above experimental results, WO_3/W film coated by four layers of $BiVO_4$ was chosen as the photoanode in the PFC system since it showed the best photoactivity. Fig. 8 shows the configuration and operation mechanism of the PFC system that comprises Pt/BJS photocathode and $BiVO_4/WO_3$/W heterojunction photoanode. For the photocathode in the established PFC, the p–n junction of the PVC plays a key role in decoupling the band bending and enhancing the photovoltage for the success of spontaneous wastewater treatment and electricity generation [38–40]. For the photoanode in the system, the formation of the heterojunction can promote efficient electron-hole separation to minimize the possibility of the energy-consuming electron-hole recombination. As shown in Fig. 8 and Fig. 1, the conduction band and valence band of $BiVO_4$ are more negative than the corresponding bands of WO_3 [35]. The thermodynamic condition favors the injection of photogenerated electrons from the conduction band of $BiVO_4$ to that of the WO_3 nanoporous film. Thus, under illumination the photogenerated electrons of $BiVO_4$ move to the WO_3 nanoporous film due to potential difference, and then the excited and exotic electrons in the WO_3 nanoporous film quickly transfer across the interface (which is part of the substrate) to the tungsten substrate due to the natural connection between them. The excited holes in the WO_3 move to the $BiVO_4$ and then migrate to the semiconductor/electrolyte interface with the holes generated in $BiVO_4$. According to the energy band theory, the Fermi level of *n*-type semiconductor lies close to its conduction band, whereas the Fermi level of *p*-type semiconductor lies close to its valence band. And the photoelectrons prefer to transfer from the photoelectrode with higher Fermi level to the lower one. As a result, the electrons transferred to the substrate then migrate to the photocathode through the external circuit due to the mismatched Fermi level.

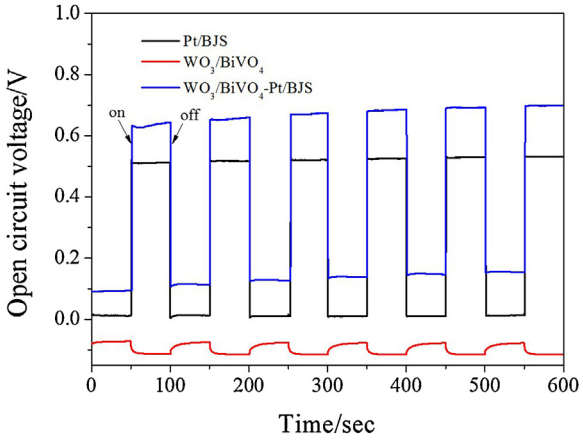

Fig. 9. The chopped V_{oc}–*t* curves of Pt/BJS photocathode, $BiVO_4/WO_3$/W photoanode and $BiVO_4/WO_3$/W–Pt/BJS system. (For interpretation of the references to color in this figure legend, the reader is referred to the web version of this article.)

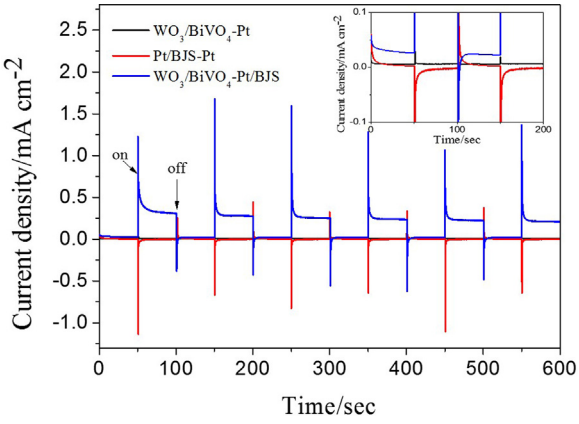

Fig. 10. The chopped J_{sc}–*t* curves of Pt/BJS photocathode, $BiVO_4/WO_3$/W photoanode and $BiVO_4/WO_3$/W–Pt/BJS system. The inset is the enlarged image for clearly determining the different curves.

In addition to the $BiVO_4/WO_3$/W–Pt/BJS system, other PFC systems composed of $BiVO_4/WO_3$/W photoanode ($BiVO_4/WO_3$/W–Pt) or Pt/BJS (Pt–Pt/BJS) photocathode alone were also established and studied under identical conditions for reference. In order to examine the photoelectric properties of all these PFC systems, both open-circuit voltage (V_{oc}) and short-circuit current (J_{sc}) density were investigated in the dark and under illumination and the results are shown in Figs. 9 and 10.

The black and red curves in Fig. 9 correspond to the V_{oc} of the Pt/BJS and the $BiVO_4/WO_3$/W systems, respectively. It was found that obvious change did not occur in the $BiVO_4/WO_3$/W system. The open circuit voltage in the dark and under light illumination were −0.07 V and −0.11 V, respectively. But significant change could be observed in the Pt/BJS system. The open circuit voltage was 0.01 V in the dark, while under illumination the value could reach 0.53 V. Based on the above results, the theoretical open circuit voltage of the $BiVO_4/WO_3$/W–Pt/BJS system under illumination can be obtained (0.64 V), which is approximately consistent with the blue curve in Fig. 9. This result indicates that the $BiVO_4/WO_3$/W–Pt/BJS system is driven by the interior bias between the two photoelectrodes.

It can be seen from the J_{sc}–*t* curves in Fig. 10 that both the Pt–Pt/BJS and the $BiVO_4/WO_3$/W–Pt systems showed the negligible response to the light illumination, which indicates that PFC based solely on the photoanode or photocathode cannot be driven for efficient water splitting. The possible reason could be that the

Table 1
Effect of the variety of substrates on PFC performance.

Organic compound	V_{oc} (V)	J_{sc} (mA cm^{-2})	Maximum power output (μW cm^{-2})	Redox potential (NHE, V)[a]
Phenol (0.05 mol L^{-1})	0.81	0.43	348.3	1.05
Glucose (0.05 mol L^{-1})	0.82	0.35	287	−0.02
Tetracycline HCl (20 mg L^{-1})	0.78	0.26	202.8	1.04
Nicotinic acid (0.05 mol L^{-1})	0.76	0.24	182.4	−0.32
Methylene blue (20 mg L^{-1})	0.78	0.29	226.2	0.20
Methyl orange (20 mg L^{-1})	0.79	0.24	189.6	0.89
Congo red (20 mg L^{-1})	0.79	0.25	197.5	0.42

[a] Measured with cyclic voltammetric method (platinum and Ag/AgCl as counter and reference electrode, respectively. 0.1 M sodium sulphate as supporting electrolyte and removal of oxygen in solution by high purity nitrogen before test. The scanning rate was 10 mV/s).

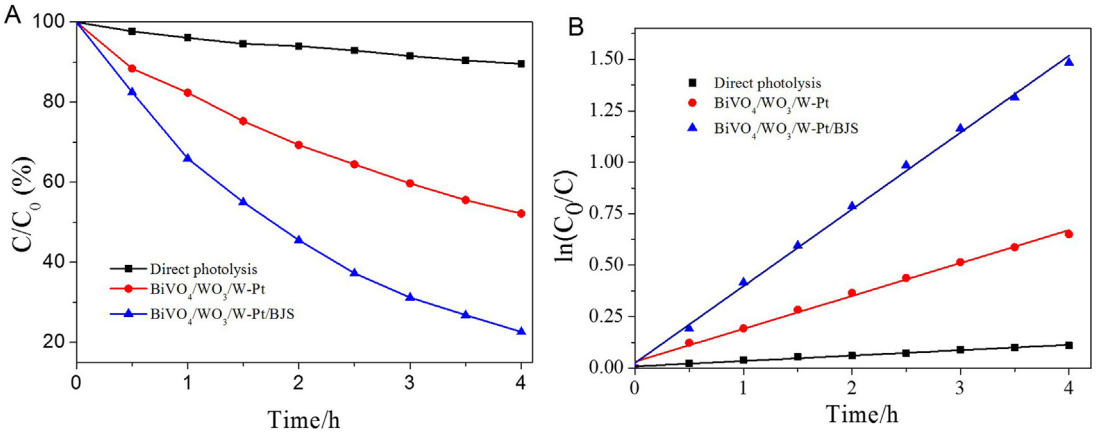

Fig. 11. (A) Degradation of tetracycline hydrochloride by direct photolysis, in WO_3/$BiVO_4$/W–Pt and WO_3/$BiVO_4$/W–Pt/BJS system, and (B) the corresponding kinetics curves.

photoanode and photocathode in the system are incapable of water reduction and oxidation because of unfavorable band voltage. In sharp contrast, under illumination the $BiVO_4$/WO_3/W–Pt/BJS system exhibited a remarkable increase in photocurrent density, which could reach and stabilize at 210 μA cm^{-2} and the transient photocurrent density could reach more than 1000 μA cm^{-2}. This result is more excellent than most of the reported visible-light responsive PFC systems such as WO_3-$GaInP_2$ system [14], WO_3/W–Cu_2O/Cu system [13] and WO_3/W–Pt/PVC system without aeration [16]. The short-circuit current density of the established PFC system is approximately twice as high as that of the WO_3/W–Pt/PVC system [15–16], which can be ascribed to the enhanced photoresponse of $BiVO_4$/WO_3/W photoanode and its excellent charge separation and transport properties [8].

3.4. Converting performance of organic compounds into electricity in the $BiVO_4$/WO_3/W-Pt/BJS PFC system

The mechanism of the PFC indicates that it can be used to degrade organic compounds due to the strong oxidizing property of the separated holes of $BiVO_4$/WO_3/W photoanode. Various model compounds (Table 1) were chosen as substrates to examine the performance of the PFC system with $BiVO_4$/WO_3/W as photoanode and Pt/BJS as photocathode and to check the simultaneous organic compounds degradation and electricity producing ability of the established PFC system. The PFC system with the introduction of phenol and glucose presented excellent cell performance. The PFC performance differences regarding to the treatment of various organic compounds may be attributed to the differences in molecular structure which will affect the degree of degradation. As can be seen from the results, the PFC system with $BiVO_4$/WO_3/W and Pt/BJS was capable of degrading various kinds of hazardous organics (e.g., phenol, tetracycline hydrochloride and various types of azo dyes) and non-toxic organics (e.g., glucose and nicotinic acid) with simultaneous electricity generation.

Tetracycline hydrochloride as a typical pollutant was chosen as the testing sample in this paper to check its long-term application for simultaneous organic compounds degradation and electricity generation. The direct photolytic, photocatalytic, and PFC-assisted photocatalytic (i.e. photoelectrocatalytic) processes of tetracycline hydrochloride solutions were performed under the given conditions. As shown in Fig. 11, the direct photolysis was clearly much slower than the other processes. Photolysis of tetracycline hydrochloride with simulated sunlight alone resulted in 10.5% tetracycline HCl removal ratio after 4 h. The presence of $BiVO_4$/WO_3/W photoanode without any external potential resulted in 48% removal ratio after 4 h. When the $BiVO_4$/WO_3/W photoanode was coupled with Pt/BJS, the tetracycline hydrochloride removal ratio sharply increased to 78%. The ranking of the rate constant k of various processes was photoelectrocatalysis (0.373 h^{-1}) > photocatalysis (0.160 h^{-1}) > direct photolysis (0.026 h^{-1}). The rate constant of photoelectrocatalysis was 2.34 times as high as that of photocatalysis, which may be ascribed to the suppression of the recombination of the photogenerated electron-hole pairs by the self-generated bias. Fig. 12 demonstrates the short-circuit current density curve of the established PFC system collected during the tetracycline hydrochloride degradation, which is relatively steady in the whole process. The consistent photocurrent confirms the stability of the PFC for long-time application.

4. Conclusions

A highly efficient $BiVO_4$/WO_3 heterojunction photoanode based on the nanoporous WO_3/W film for visible-light responsive dual photoelectrode PFC was reported in this paper. The optimized $BiVO_4$/WO_3/W photoanode obtained a photocurrent of 2.01 mA/cm^2 at 0.6 V (vs Ag/AgCl) in 0.1 M KH_2PO_4 (pH 7) electrolyte under simulated AM1.5 solar light, which was 180% and 205% higher than that of bare WO_3 film and bare $BiVO_4$ film,

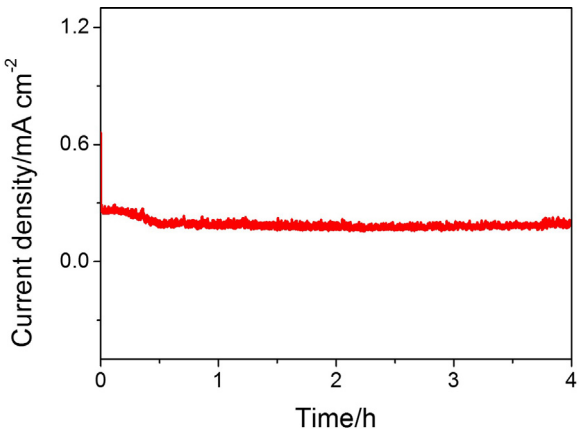

Fig. 12. Variation of current of the PFC system in a typical process of tetracycline hydrochloride degradation.

respectively, and it was coupled with Pt/BJS photocathode to form a visible-light responsive dual photoelectrode PFC which showed high converting performance of organics into electricity.

Acknowledgements

The authors are grateful for financial support provided by the National Nature Science Foundation of China (No. 21207088, No. 21177085, No. 21276153, No. 51578332) and the Shanghai Yangfan Program (14YF1401500).

References

[1] Y. Feng, H. Lee, X. Wang, Y. Liu, W. He, Bioresour. Technol. 101 (2010) 632–638.
[2] N. Strataki, M. Antoniadou, V. Dracopoulos, P. Lianos, Catal. Today 151 (2010) 53–57.
[3] Y. Liu, J. Li, B. Zhou, X. Li, H. Chen, Q. Chen, Z. Wang, L. Li, J. Wang, W. Cai, Water Res. 45 (2011) 3991–3998.
[4] Y.B. Liu, J.H. Li, B.X. Zhou, H.C. Chen, Z.S. Wang, W.M. Cai, Chem. Commun. 47 (2011) 10314–10316.
[5] Y. Liu, J. Li, B. Zhou, S. Lv, X. Li, H. Chen, Q. Chen, W. Cai, Appl. Catal. B: Environ. 111–112 (2012) 485–491.
[6] M. Antoniadou, P. Lianos, Photochem. Photobiol. Sci. 10 (2011) 431–435.
[7] J. Li, J. Li, Q. Chen, J. Bai, B. Zhou, J. Hazard. Mater. 262 (2013) 304–310.
[8] Z. Wu, G. Zhao, Y. Zhang, J. Liu, Y. Zhang, H. Shi, J. Mater. Chem. A 3 (2015) 3416–3424.
[9] D. Meissner, B. Memming, R. Kastening, J. Phys. Chem 92 (1988) 3476–3483.
[10] Q. Zeng, J. Bai, J. Li, Y. Li, X. Li, B. Zhou, Nano Energy 9 (2014) 152–160.
[11] Y. Liu, H. Zhou, B. Zhou, J. Li, H. Chen, J. Wang, J. Bai, W. Shangguan, W. Cai, Int. J. Hydrogen Energy 36 (2011) 167–174.
[12] Y. Liu, H. Zhou, J. Li, H. Chen, D. Li, B. Zhou, W. Cai, Nano-Micro Lett. 2 (2010) 277–284.
[13] Q. Chen, J. Li, X. Li, K. Huang, B. Zhou, W. Cai, W. Shangguan, Environ. Sci. Technol. 46 (2012) 11451–11458.
[14] H. Wang, J.A. Turner, J. Electrochem. Soc. 157 (2010) F173–F178.
[15] Q. Chen, J. Li, X. Li, K. Huang, B. Zhou, W. Shangguan, ChemSusChem 6 (2013) 1276–1281.
[16] Q. Chen, J. Bai, J. Li, K. Huang, X. Li, B. Zhou, W. Cai, Chem. Eng. J. 252 (2014) 89–94.
[17] J. Yang, W. Liao, Y. Liu, M. Murugananthan, Y. Zhang, Electrochim. Acta 144 (2014) 7–15.
[18] Q. Liu, Q. Chen, J. Bai, J. Li, J. Li, B. Zhou, J. Solid State Electrochem. 18 (2014) 157–161.
[19] J.Y. Kim, D.H. Youn, J.H. Kim, H.G. Kim, J.S. Lee, ACS Appl. Mater. Interfaces 7 (2015) 14123–14129.
[20] K. Zhang, X. Shi, J.K. Kim, J.S. Lee, J.H. Park, Nanoscale 5 (2013) 1939–1944.
[21] Y. Park, K.J. McDonald, K.-S. Choi, Chem. Soc. Rev. 42 (2013) 2321–2337.
[22] W.J. Jo, J.-W. Jang, K.-J. Kong, H.J. Kang, J.Y. Kim, H. Jun, K.P.S. Parmar, J.S. Lee, Angew. Chem. Int. Ed. 51 (2012) 3147–3151.
[23] Ho-Kimura, S.J.A. Moniz, A.D. Handoko, J. Tang, J. Mater. Chem. A 2 (2014) 3948–3953.
[24] F.F. Abdi, R. van de Krol, J. Phys. Chem. C 116 (2012) 9398–9404.
[25] Y. Liang, T. Tsubota, L.P.A. Mooij, R. van de Krol, J. Phys. Chem. C 115 (2011) 17594–17598.
[26] E.S. Kim, H.J. Kang, G. Magesh, J.Y. Kim, J.-W. Jang, J.S. Lee, ACS Appl. Mater. Interfaces 6 (2014) 17762–17769.
[27] S.J.A. Moniz, J. Zhu, J. Tang, Adv. Energy Mater. 4 (2014) 1301590.
[28] L. Zhang, E. Reisner, J.J. Baumberg, Energy Environ. Sci. 7 (2014) 1402–1408.
[29] P.M. Rao, L. Cai, C. Liu, I.S. Cho, C.H. Lee, J.M. Weisse, P. Yang, X. Zheng, Nano lett. 14 (2014) 1099–1105.
[30] J. Su, L. Guo, N. Bao, C.A. Grimes, Nano lett. 11 (2011) 1928–1933.
[31] R. Saito, Y. Miseki, K. Sayama, Chem. Commun. 48 (2012) 3833–3835.
[32] M.G. Mali, H. Yoon, M.-w. Kim, M.T. Swihart, S.S. Al-Deyab, S.S. Yoon, Appl. Phys. Lett. 106 (2015) 151603.
[33] P. Chatchai, Y. Murakami, S.-y. Kishioka, A.Y. Nosaka, Y. Nosaka, Electrochim. Acta 54 (2009) 1147–1152.
[34] I. Fujimoto, N. Wang, R. Saito, Y. Miseki, T. Gunji, K. Sayama, Int. J. Hydrogen Energy 39 (2014) 2454–2461.
[35] S.J. Hong, S. Lee, J.S. Jang, J.S. Lee, Energy Environ. Sci. 4 (2011) 1781–1787.
[36] J.H. Kim, G. Magesh, H.J. Kang, M. Banu, J.H. Kim, J. Lee, J.S. Lee, Nano Energy 15 (2015) 153–163.
[37] Q. Jiaa, K. Iwashinaa, A. Kudo, Pros. Natl. Acad. Sci. U. S. A. 109 (2012) 11564–11569.
[38] I. Lombardi, S. Marchionna, G. Zangari, S. Pizzini, Langmuir 23 (2007) 12413–12420.
[39] R.N. Dominey, N.S. Lewis, J.A. Bruce, D.C. Bookbinder, M.S. Wrighton, J. Am. Chem. Soc. 104 (1982) 467–482.
[40] S.W. Boettcher, E.L. Warren, M.C. Putnam, E.A. Santori, D. Turner-Evans, M.D. Kelzenberg, M.G. Walter, J.R. McKone, B.S. Brunschwig, H.A. Atwater, N.S. Lewis, J. Am. Chem. Soc. 133 (2011) 1216–1219.